Available online at www.sciencedirect.com

ScienceDirect

Advances in Space Research xxx (xxxx) xxx

ADVANCES IN SPACE RESEARCH (a COSPAR publication)

www.elsevier.com/locate/asr

BDS-2/BDS-3 uncalibrated phase delay estimation considering the intra-system bias

Yangfei Hou [a,b,c], Yize Zhang [c,*], Junping Chen [c,d], Lizhen Lian [c], Jiexian Wang [a]

[a] College of Surveying and Geo-informatics, Tongji University, Shanghai 200092, China
[b] Shanghai Key Laboratory of Space Navigation and Positioning Techniques, Shanghai 200030, China
[c] Shanghai Astronomical Observatory, Chinese Academy of Sciences, Shanghai 200030, China
[d] School of Astronomy and Space Science, University of Chinese Academy of Sciences, Beijing 100049, China

Received 3 July 2022; received in revised form 8 October 2022; accepted 17 October 2022

Abstract

Intra-system biases (ISBs) between BDS-2 and BDS-3 are of critical importance when combining observations from the BDS-2 and BDS-3 systems, which is meaningful to fully take advantage of the BDS positioning capability. Meanwhile, ISBs should also be considered in the estimation of BDS uncalibrated phase delays (UPDs). In this research, we present a BDS-2/BDS-3 joint-processing scheme, as well as a method for estimating BDS UPDs. The characteristics of ISBs and the quality of BDS UPDs are analyzed based on 30-day data from 130 multi-GNSS experimental (MGEX) stations. Our results indicate that the ISBs are related to the type and version of the receiver. The ISBs can be regarded as constant across the course of a given day, and the mean standard deviation (STD) values of ISBs over one month for different types of receivers are generally within 0.2 m. Moreover, to assess the quality of UPD products, the residuals of the estimated UPDs and the utilization rates of the observation data are computed. The results show that the quality of BDS UPDs can be improved by correcting the satellite-induced pseudo-range variations, and by estimating the wide-lane (WL) UPD difference between BDS-2 and BDS-3. The average RMS values of the estimated residuals of WL UPD and narrow-lane (NL) UPD are 0.07 and 0.09 cycles, respectively; moreover, the utilization rate of the observation data of WL UPD and NL UPD can reach above 90 %. The performance of BDS precise point positioning (PPP) and PPP ambiguity resolution (PPP-AR) is analyzed in terms of positioning accuracy and convergence performance in both the static and kinematic modes. Compared with PPP ambiguity-float solutions, the positioning accuracy of PPP-AR is significantly improved, especially in the east direction. The impact of ISBs on PPP and PPP-AR is also analyzed, and the results indicate that ISBs can improve the convergence speed of float PPP, but can be disregarded in PPP-AR.

Keywords: BDS-2+BDS-3; ISB; UPD; PPP-AR

1. Introduction

The second phase of China's navigation satellite system (BDS-2) has provided regional service in the Asia-Pacific area since 27 December 2012; the third generation of the system, BDS-3, began to provide global service at the end of 2018 (Yang et al., 2020). At present, BDS-2 consists of fifteen satellites, including three medium earth orbit (MEO) satellites, seven inclined geosynchronous orbit (IGSO) satellites, and five geostationary earth orbit (GEO) satellites. Meanwhile, BDS-3 has 30 satellites, including 3 GEO satellites, 3 IGSO satellites, and 24 MEO satellites. These BDS-2 satellites transmit signals on three frequencies: B1I (1561.098 MHz), B2I (1207.14 MHz), and B3I (1268.52 MHz) (Yang et al., 2011). For BDS-3, the satellites transmit the original BII and B3I signals, and the new B1C (1575.42 MHz), B2a

* Corresponding author.
E-mail address: zhyize@shao.ac.cn (Y. Zhang).

https://doi.org/10.1016/j.asr.2022.10.041
0273-1177/

(1176.45 MHz), B2b (1207.14 MHz), and B2ab (1191.795 MHz) signals. BDS-2 and BDS-3 have overlapping signal frequencies, and BDS-2/BDS-3 joint processing is normally utilized on B1I and B3I, which increases the number of visible satellites (Meng et al., 2020) and improves the BDS performance.

Precise point positioning (PPP) is a technique used to obtain high-precision coordinates by using pseudo-range and phase observations from a single receiver (Kouba and Heroux, 2001, Zumberge et al., 1997). Up to the present, it has been widely used in fields such as deformation monitoring, atmospheric monitoring, and unmanned driving. In recent years, many studies have begun to focus on BDS-2 and BDS-3 joint positioning. Zhang et al. (2019) found that the convergence time of the BDS kinematic PPP could be reduced when combining BDS-2 and BDS-3. Chen et al. (2022) found that the performance of BDS-2 and BDS-3 in combination is superior to that of BDS-2-only constellations. In these studies, the intra-system bias (ISB) between BDS-2 and BDS-3 are not considered when evaluating the joint processing, and the BDS-2 and BDS-3 systems are treated as though they were the same system. In fact, BDS-2 and BDS-3 were built independently and the processing strategy of the two systems are not the same; the receiver code hardware delay of BDS-2 is also different from that of BDS-3 (Jiao et al., 2020; Qin et al., 2020). Zhao et al. (2020) found that the introduction of ISB between BDS-2 and BDS-3 can improve the performance of BDS joint PPP. Chen et al. (2021) evaluated both the static and kinematic BDS joint-PPP performance, and the results show that the ISB should be considered in the PPP. Shi et al. (2022) investigated the temporal and long-term characteristics ISB and conclude that the ISB between BDS-2 and BDS-3 should be considered in BDS-2/BDS-3 joint models. Hence, the influence of ISB on joint BDS-2 and BDS-3 PPP ambiguity resolution (PPP-AR) also needs to be further studied.

PPP users usually adopt integer clock (Collins et al., 2008; Laurichesse et al., 2009) or uncalibrated phase delay (UPD) products (Ge et al., 2008; Geng et al., 2012) to recover the characteristics of integer ambiguity. Over the last ten years, PPP-AR has developed from GPS to multi-GNSS, various institutions and analysis centers of the International GNSS Service (IGS) provide satellite products to users to achieve PPP-AR (Glaner and Weber, 2021). The integer clock or UPD products currently available to implement BDS PPPAR include Centre national d'études spatiales (CNES), Center for Orbit Determination in Europe (CODE), GBM, School of Geodesy and Geomatics (SGG) and the PRIDE Lab at Wuhan University (WHU). Some scholars have analyzed the performance of BDS PPP-AR. Liu et al. (2019) found that the introduction of the BDS-2 system in PPP-AR can significantly shorten the time to first fix of multi-GNSS PPP-AR. Qu et al. (2019) and Li et al. (2020) investigated the combination of BDS-2 and BDS-3 PPP-AR. The results show that the coordinates precision for ambiguity-fixed solutions are significantly improved. However, in these studies, the receiver bias between BDS-2 and BDS-3 satellites was not considered. Hu et al. (2022) evaluated the impact of ISB parameters on the BDS UPD estimation results and showed that estimating ISB can improve the BDS UPD quality. In addition, it was found that BDS-2 satellites have satellite-induced code pseudo-range variations (Lou et al., 2017; Wanninger et al., 2015), and the influence of this deviation on BDS PPP-AR also requires further analysis.

Based on the matters addressed above, we focus on three issues in this research. Firstly, the ISB characteristics between BDS-2 and BDS-3 are analyzed based on 30-day data. Secondly, we evaluate the influence on BDS UPD estimation of both BDS satellite-induced code pseudo-range variations, and the receiver hardware delay between BDS-2 and BDS-3. Finally, the performance of BDS PPP and PPP-AR are analyzed in terms of positioning accuracy and convergence performance.

2. Methodology

2.1. PPP float solution

The Ionosphere-free (IF) combination model and uncombined model can be used to eliminate the first-order ionospheric delays in the code and carrier-phase measurements (Lou et al., 2016; Boisits et al., 2020). The conventional IF code $P^s_{r,IF}$ and carrier-phase $L^s_{r,IF}$ can be written as.

$$P^s_{r,IF} = \rho^s_r + c\cdot dt_r - c\cdot dt^s + M^s\cdot zwd_r + b_{r,P_{IF}} - b^s_{P_{IF}} + e^s_{r,IF} \quad (1)$$

$$L^s_{r,IF} = \rho^s_r + c\cdot dt_r - c\cdot dt^s + M^s\cdot zwd_r + b_{r,L_{IF}} - b^s_{L_{IF}} + \lambda_{IF}\cdot N^s_{r,IF} + \varepsilon^s_{r,IF} \quad (2)$$

where ρ^s_r is the geometrical propagation distance between the satellite and receiver; c is the speed of light; dt_r and dt^s are the receiver and satellite clock errors, respectively; zwd_r and M^s are the wet zenith tropospheric delay and its mapping function, respectively; $b_{r,P_{IF}}$ and $b^s_{P_{IF}}$ are the code hardware delays of the IF observation for the receiver and satellite, respectively; $b_{r,L_{IF}}$ and $b^s_{L_{IF}}$ are the IF carrier phase hardware delays for the receiver and satellite, respectively; λ_{IF} is the wavelength of IF phase observations; and $N^s_{r,IF}$ is the phase ambiguity. $e^s_{r,IF}$ and $\varepsilon^s_{r,IF}$ are the noise of IF pseudo-range and carrier-phase observations, respectively.

In general, the IF model is used to estimate the satellite clock error in IGS precise products. However, the hardware delay, clock error, and phase ambiguity are correlated and cannot be separated. Hence, the code and phase hardware delay is absorbed by clock errors and ambiguities, respectively. Equations (1) and (2) can be expressed as:

$$P^s_{r,IF} = \rho^s_r + c\cdot \bar{dt}_r - c\cdot \bar{dt}^s + M^s\cdot zwd_r + e^s_{r,IF} \quad (3)$$

$$L^s_{r,IF} = \rho^s_r + c\cdot d\bar{t}_r - c\cdot d\bar{t}^s + M^s\cdot zwd_r + \lambda_{IF}\cdot \bar{N}^s_{r,IF} + \varepsilon^s_{r,IF} \quad (4)$$

Further$d\bar{t}_r d\bar{t}^s$, and $\bar{N}^s_{r,IF}$ are as follows:

$$c\cdot d\bar{t}_r = c\cdot dt_r + b_{r,P_{IF}} \quad (5)$$

$$c\cdot d\bar{t}^s = c\cdot dt^s + b^s_{P_{IF}} \quad (6)$$

$$\lambda_{IF}\cdot \bar{N}^s_{r,IF} = \lambda_{IF}\cdot N^s_{r,IF} + (b_{r,L_{IF}} - b^s_{L_{IF}}) - (b_{r,P_{IF}} - b^s_{P_{IF}}) \quad (7)$$

In the process of BDS joint PPP, the BDS-2 and BDS-3 precise clock use different reference. Meanwhile, the receiver hardware delay also differs between BDS-2 and BDS-3. To study the characteristic of ISBs between BDS-2 and BDS-3, the IF combinations of BDS-2 and BDS-3 can be described as follows:

$$P^{s\ominus 2}_{r,IF} = \rho^{s\ominus 2}_r + c\cdot d\bar{t}^{-3}_r - c\cdot d\bar{t}^{s,2} + M^s\cdot zwd^2_r + ISB + e^{s,2}_{r,IF} \quad (8)$$

$$L^{s,2}_{r,IF} = \rho^{s,2}_r + c\cdot d\bar{t}^{-3}_r - c\cdot d\bar{t}^{s,2} + M^s\cdot zwd^2_r + \lambda_{IF}\cdot \bar{N}^{s,2}_{r,IF} + ISB + \varepsilon^{s,2}_{r,IF} \quad (9)$$

$$P^{s,3}_{r,IF} = \rho^{s,3}_r + c\cdot d\bar{t}^{-3}_r - c\cdot d\bar{t}^{s\ominus 3} + M^s\cdot zwd^3_r + e^{s,3}_{r,IF} \quad (10)$$

$$L^{s,3}_{r,IF} = \rho^{s,3}_r + c\cdot d\bar{t}^{-3}_r - c\cdot d\bar{t}^{s,3} + M^s\cdot zwd^3_r + \lambda_{IF}\cdot \bar{N}^{s,3}_{r,IF} + \varepsilon^{s,3}_{r,IF} \quad (11)$$

where $d\bar{t}^{-3}_r$ and $d\bar{t}^{s\ominus 3}$ are the receiver and satellite clock of BDS-3, and $d\bar{t}^{s\ominus 2}$ s the satellite clock error of BDS-2. The ISB parameter mainly contains the clock bias and the receiver code hardware delay between BDS-2 and BDS-3. Since the BDS-3 satellites are globally visible, the receiver clock error of BDS-3 is chosen as the clock reference in Eq. (8) to (11). Moreover, the difference between BDS-2 and BDS-3 precise clock bias is a stable value within a day (Shi et al., 2022; Chen et al., 2020). Therefore, we mainly focus on analyzing the relationship between the receiver hardware delay and ISBs.

In addition, BDS-2 satellites were found to have satellite-induced code pseudo-range variations that can be corrected according to Eq. (12), which can be expressed as.

$$MP = a_1\cdot E\mathrm{le} + a_2\cdot Ele^2 + a_3\cdot Ele^3 \quad (12)$$

where MP is the variation and Ele is the elevation angle; the polynomial coefficientsa_1, a_2 and a_3 are listed in Table 1.

Table 1
BDS pseudo-range deviation correction coefficient (Lou et al., 2017) (Unit: m).

Coefficient	IGSO			MEO		
	B1	B2	B3	B1	B2	B3
a_1	−0.59	−0.26	−0.10	−0.95	−0.60	−0.20
a_2	1.62	1.00	0.75	2.16	1.64	0.65
a_3	−0.64	−0.38	−0.31	−0.64	−0.57	−0.18

2.2. PPP ambiguity-fixed solution

From section2.1, the effect of the ISB parameter needs to be considered when performing UPD product estimation. The BDS WL UPD can be separated from the ambiguity parameters. The float WL ambiguity can be resolved with the Melbourne–Wübbena (MW) linear combination observation (Melbourne, 1985; Wübbena, 1985).

$$\bar{N}^{s,2}_{r,WL} = N^{s,2}_{r,WL} + UPD^2_{r,WL} - UPD^{s,2}_{WL} \quad (13)$$

$$\bar{N}^{s,3}_{r,WL} = N^{s,3}_{r,WL} + UPD^3_{r,WL} - UPD^{s,3}_{WL} \quad (14)$$

where $\bar{N}^{s,*}_{r,WL}$ and $N^{s,*}_{r,WL}$ are the float and integer WL ambiguity, respectively; $UPD^*_{r,WL}$ and $UPD^{s,*}_{WL}$ are the receiver and satellite UPDs, respectively. Geng et al. (2019a) and Geng et al. (2019b) enable tightly coupled inter-GNSS PPP-AR by calibrating station-specific inter-system phase bias (ISPB) between different GNSS systems, the results show that the inter-GNSS PPPAR is superiority to intra-GNSS PPP-AR. Similarly, to ensure the consistency of WL UPDs for receivers, it is necessary to estimate a WL UPD difference between BDS-2 and BDS-3, and this can be expressed as:

$$R^{s,2}_r = UPD^3_{r,WL} - UPD^{s,2}_{WL} + UPD^{2-3}_{r,WL} \quad (15)$$

$$R^{s,3}_r = UPD^3_{r,WL} - UPD^{s,3}_{WL} \quad (16)$$

where $R^{s,*}_r$ is the fractional part of the float WL ambiguity, and $UPD^{2-3}_{r,WL}$ is the WL UPD difference between BDS-2 and BDS-3. For a network with n stations tracking m satellites, the observation equation for the ambiguities can be written as:

$$\begin{bmatrix} R^1_1 \\ \vdots \\ R^m_1 \\ \vdots \\ R^m_n \end{bmatrix} = \begin{bmatrix} 1 & \cdots & 1 & \cdots & -1 & \cdots \\ \vdots & \vdots & \vdots & \vdots & \vdots & \vdots \\ 1 & \cdots & 0 & \cdots & \cdots & -1 \\ \vdots & \vdots & \vdots & \vdots & \vdots & \vdots \\ \vdots & \vdots & \vdots & \vdots & \vdots & \vdots \\ \cdots & 1 & \cdots & \cdots & \cdots & 1 \end{bmatrix} \begin{bmatrix} UPD^3_{1,WL} \\ \vdots \\ UPD^{2-3}_{1,WL} \\ \vdots \\ UPD^1_{WL} \\ \vdots \\ UPD^m_{WL} \end{bmatrix} \quad (17)$$

The WL UPD can be estimated through the least-square adjustment, while the normal equation is rank deficiency because of the linear dependency between the satellite and receiver UPDs. This issue can be solved by constraining the sum of satellite UPDs and sum of WL UPD difference between BDS-2 and BDS-3 as zero.

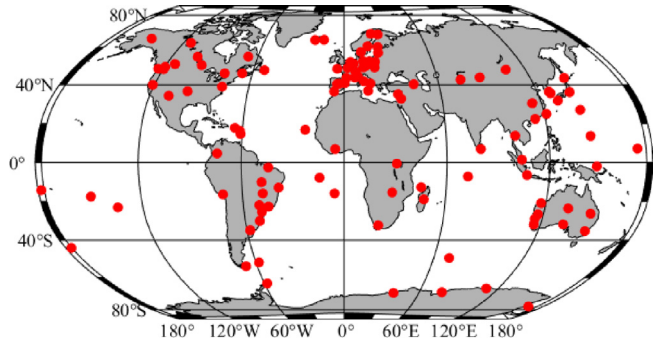

Fig. 1. Distribution of 130 selected MGEX stations for BDS ISB and UPD estimation.

After correcting the WL ambiguities with the WL UPDs, they can be fixed to integers. The float NL ambiguity can be described as follows:

$$\tilde{N}^{s}_{r,Nl} = \frac{f_1 + f_2}{f_1}\tilde{N}^{s}_{r,IF} - \frac{f_2}{f_1 - f_2}N^{s}_{r,WL} \tag{18}$$

where $\tilde{N}^{s}_{r,IF}$ is the float ambiguity of the ionosphere-free combination;$N^{s}_{r,WL}$ is the integer WL ambiguity; and $\tilde{N}^{s}_{r,NL}$ is the float NL ambiguity. The NL UPDs can be formulated as.

$$\bar{N}^{s}_{r,NL} = N^{s}_{r,NL} + UPD_{r,NL} - UPD^{s}_{NL} \tag{19}$$

The same approach can be used to estimate the NL UPDs from the derived float NL ambiguities. In this paper, the bootstrap method is applied to fix the WL ambiguities, while the partial searched strategy based on the LAMBDA method is used to fix the NL ambiguities (Li et al., 2013; Teunissen, 2002; Xiao et al., 2019).

For the server side of PPP-AR, the WL UPD difference between BDS-2 and BDS-3 should be provide to user for WL ambiguities fixing. Since the receiver-side UPD of BDS-3 was chosen as the reference, the satellite of BDS-3 with the highest elevation also is selected as the reference satellite when performing PPP-AR. For the user side PPP-AR, the WL UPD difference between BDS-2 and BDS-3 is provided to the user if the user's receiver type is the same as server stations. For the user site whose BDS-2 and BDS-3 WL UPD difference is not known, it is better to regard BDS-2 and BDS-3 as two systems when performing PPP-AR, and the user need to select the reference satellite for BDS-2 and BDS-3 separately.

3. Analysis of ISB characteristics

In the joint data processing of the BDS-2 and BDS-3 overlapping frequencies, the results are affected by the ISBs between BDS-2 and BDS-3, so the characteristics of ISBs need to be distinguished. In this section, the temporal

Table 2
Receiver information for the selected MGEX stations.

Receiver	Model	Number	Note
JAVAD	JAVAD TRE_3 JAVAD TRE_3 DELTA	25	Tracks C19 ~ C30, C32 ~ C46
TRIMBLE	ALLOY NETR9	40	Tracks C19 ~ C30, C32 ~ C46
SEPTENTRIO	POLARX5 POLARX5TR	55	Tracks C19 ~ C30, C32 ~ C46
LEICA	GR50 GR30	10	Cannot track the B3I signal

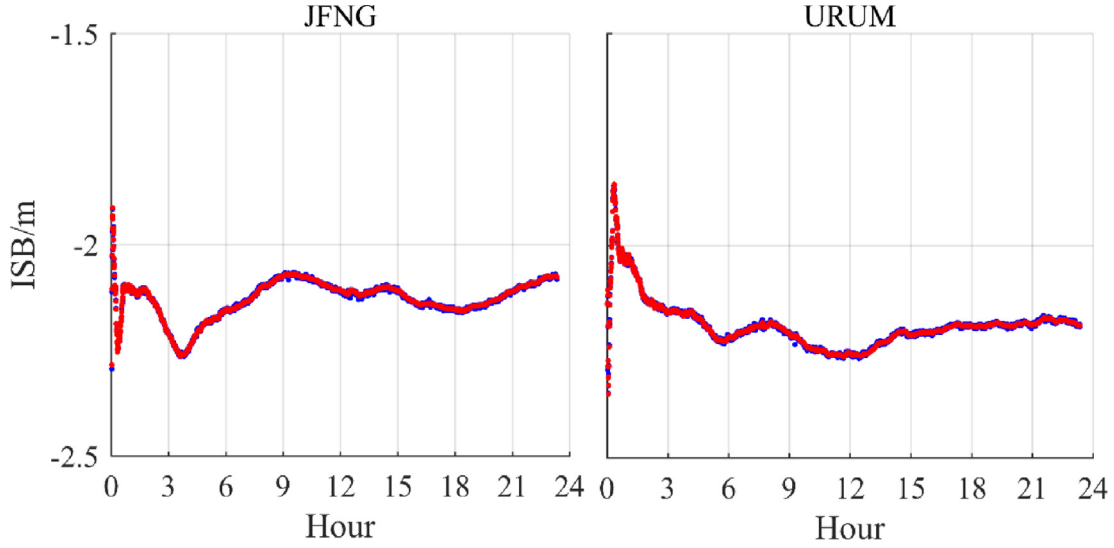

Fig. 2. Time series of BDS ISB using WN and RW estimation strategies, respectively.

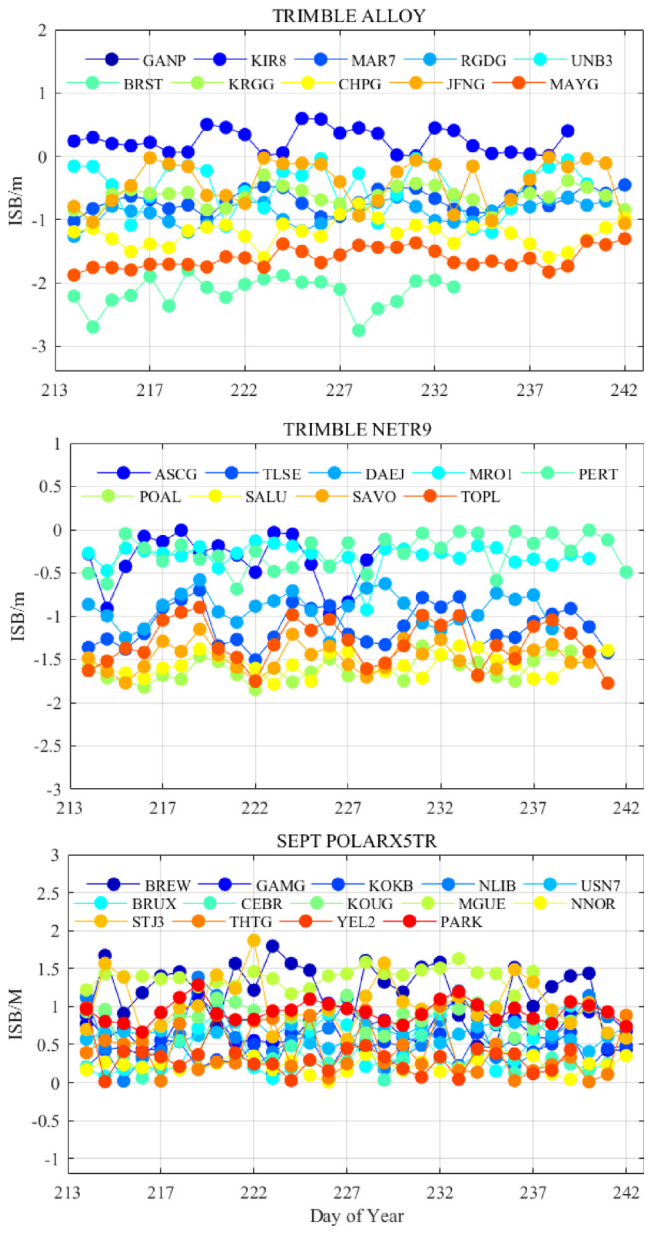

Fig. 3. Top to bottom: ISB series of TRIMBLE ALLOY, TRIMBLE NETR9, and SEPT POLARX5TR, respectively, during DOY 213–242, 2021.

and long-term characteristics of ISBs between BDS-2 and BDS-3 are analyzed.

3.1. Experimental data

At present, about 160 MGEX stations have the ability to track BDS-2 and BDS-3 signals. To ensure the reliability of BDS-2 and BDS-3 joint processing, we delete some stations with insufficient number of BDS-3 satellites, and 130 globally distributed MGEX stations are selected for the estimation of ISBs and UPDs. The distribution of these stations is shown in Fig. 1, and data from the DOY 213 to 242 in 2021 are collected in a 30 s sampling interval. Both the precise clock with a sampling interval of the 30 s and the orbit products are from WHU.

Details of the receivers equipped at the above stations are given in Table 2. There are eight different receiver types: JAVAD TRE_3, JAVAD TRE_3 DELTA, TRIMBLE ALLOY, TRIMBLE NETR9, SEPTENTRIO POLARX5, SEPTENTRIO POLARX5TR, LEICA GR50, and LEICA GR30.

3.2. ISB short-term characteristic analysis

Since the characteristics of ISBs are uncertain, the ISBs can be estimated as white noise (WN) or rand walk (RW) parameters (Chen et al., 2015; Zhou et al., 2019; Song et al.,2020). In this paper, the data of JFNG (TRIMBLE ALLOY) on DOY 213, 2021, and URUM (JAVAD TRE_3) on DOY 222, 2021, are selected to estimate the ISB parameter. Fig. 2 displays the ISB series of JFNG and URUM. The blue line represents the WN result, while the red one represents the RW result.

Fig. 2 shows that the ISB value of each station is not zero, showing the presence of ISBs between BDS-2 and BDS-3. In addition, the ISBs estimated by the WN strategies are close to those estimated by the RW strategies, and the ISB series remain stable after convergence. That is to say, the ISBs can be considered a constant value across the course of a day.

3.3. ISB long-term characteristic analysis

To investigate the long-term ISB characteristics, observations from 70 MGEX stations with different receiver types, such as TRIMBLE, SEPT, and JAVAD, are selected to estimate the ISBs from DOY 213 to 242, 2021.

Fig. 3 gives the 30-day ISB series of TRIMBLE ALLOY (10 stations), TRIMBLE NETR9 (9 stations), and SEPT POLARX5TR (14 stations), respectively. Each color in the figure represents the mean ISB value of one day. The ISB values of most stations vary within 0.5 m over 30 days. The ISB is stable in terms of long-term varying characteristics. In addition, it can be seen from Fig. 3 that the ISB values for different receiver types are different. As shown in Fig. 3, the ISB values of TRIMBLE NETR9 and SEPT POLARX5TR vary from −2 to 0 m, and 0 to 2 m, respectively. The ISB values of TRIMBLE ALLOY are within 3.8 m, which is a range larger than that of other receiver types.

The ISB series of SEPT POLARX5 (19 stations) and JAVAD TRE_3 DELTA (18 stations) are shown in Fig. 4, from DOY 213 to 242, 2021. It can be seen from Fig. 4 that the ISB is stable in terms of long-term characteristics, and it is related to the receiver types. Most of the ISB values for the same type of receiver in Fig. 4 are less discrete than the receivers in Fig. 3, but two stations have a unique result compared to the other stations. It is confirmed that one station is MAO0 with the receiver type SEPT POLARX5 (version:5.4.0), and the other station is BOGT with the receiver type JAVAD TRE_3 DELTA

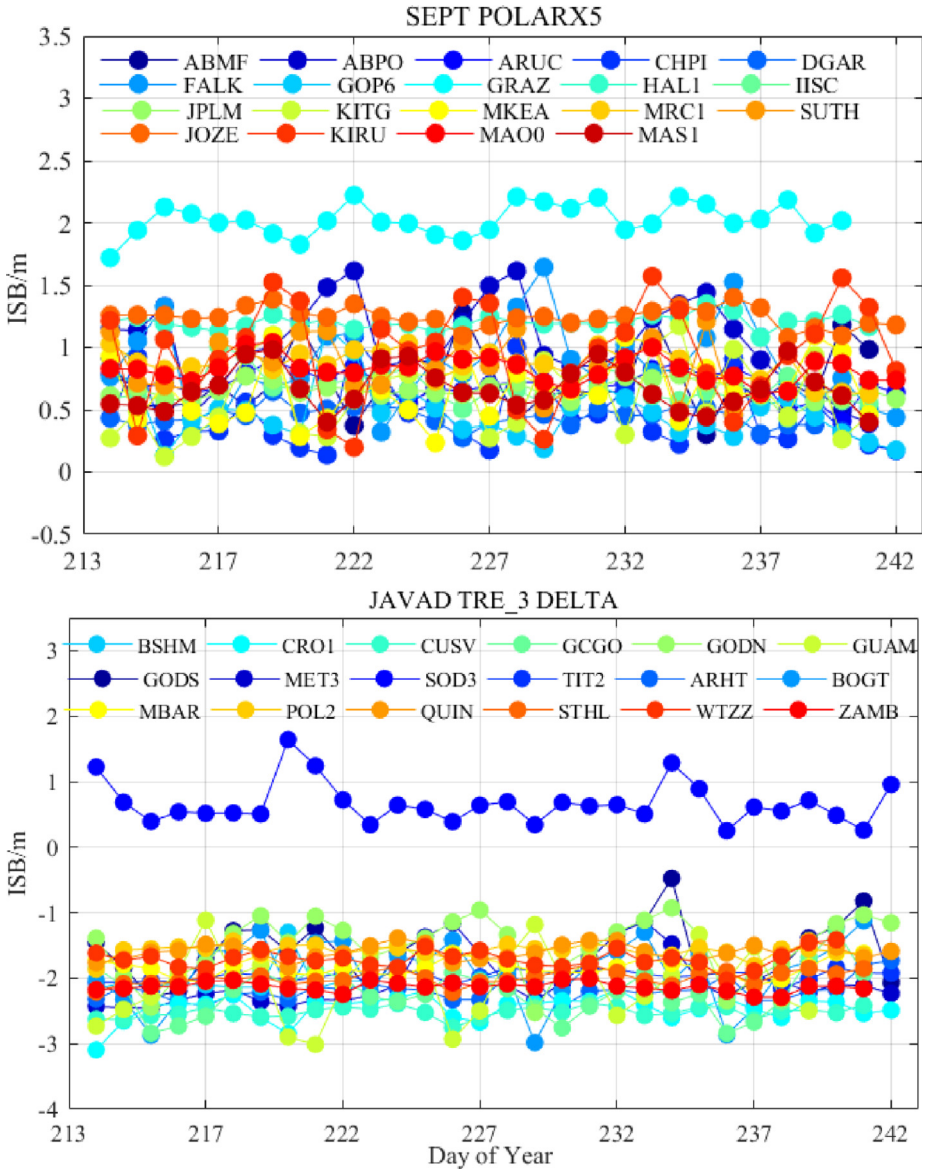

Fig. 4. ISB series of SEPT POLARX5 and JAVAD TRE_3 DELTA, respectively, during DOY 213–242, 2021.

(version:4.1.01). Although the receiver type of these two stations is the same as that of the other stations, the version number is different. This indicates that the ISB is not only related to the receiver types but also related to the receiver version. According to Fig. 4, except for the stations MAO0 and BOGT, the ISB values of SEPT POLARX5 and JAVAD TRE_3 DELTA range from 0 to 1.7 m, and −3 to −0.4 m, respectively.

Fig. 5 gives the 30-day ISB STD values of different stations, which represent the long-term ISB stability. It shows that the 30-day ISB STD of most stations is within 0.2 m, and the maximum value is also within 0.3 m.

4. Quality assessment of BDS UPD products on the network side

The quality and accuracy of satellite UPDs have a significant impact on PPP-AR performance. In this section, the quality of the BDS UPDs is assessed from the perspectives of the residuals of the UPD solutions, and the data utilization rate of each BDS satellite.

As shown in Table 3, three methods of data processing are performed and compared. For Solution A, the satellite-induced code pseudo-range variations are not corrected, and the $UPD^{2-3}_{r,WL}$ and ISBs are not estimated. Solution B corrects for the satellite-induced code pseudo-range variations, but the $UPD^{2-3}_{r,WL}$ and ISBs are not estimated. For Solution C, the satellite-induced code pseudo-range variations are corrected, and the $UPD^{2-3}_{r,WL}$ and ISB are estimated.

4.1. Results of WL UPD

Firstly, the WL UPDs estimated by the three strategies are evaluated to analyze the impact of two factors on the BDS WL UPD results: namely, the satellite-induced code

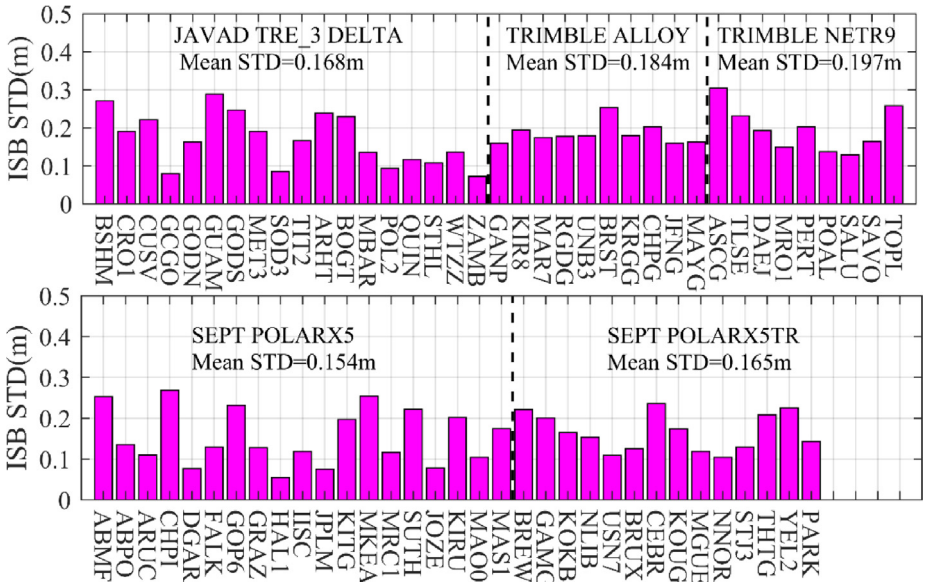

Fig. 5. STD value of ISB series at each station during DOY 213–242 in 2021.

Table 3
List of data-processing methods.

Methods	Details
Solution A	Satellite-induced code pseudo-range variations without correction; $UPD^{2-3}_{r,WL}$ and ISB without estimation
Solution B	Satellite-induced code pseudo-range variations with correction; $UPD^{2-3}_{r,WL}$ and ISB without estimation
Solution C	Satellite-induced code pseudo-range variations with correction; $UPD^{2-3}_{r,WL}$ and ISB with estimation

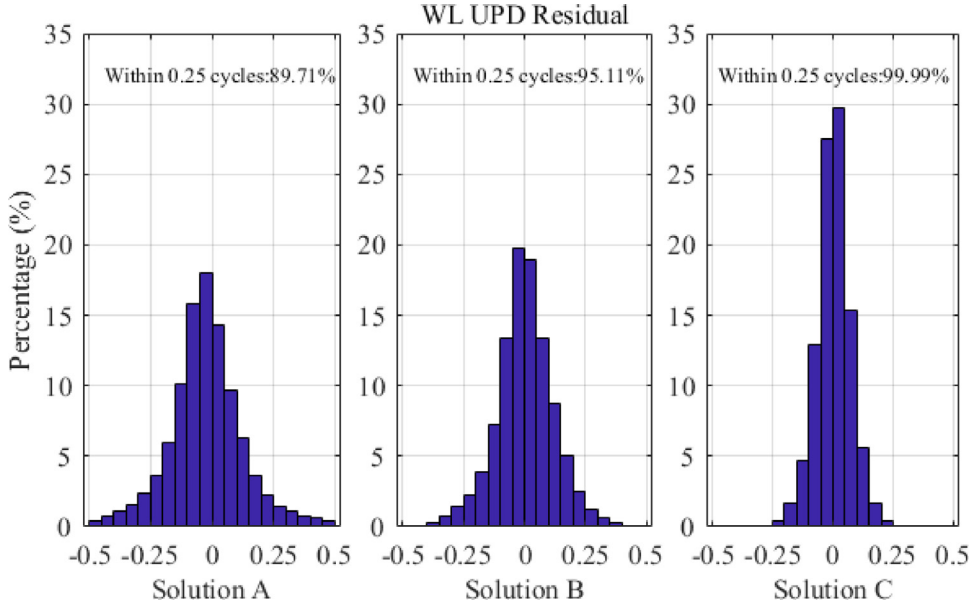

Fig. 6. Histogram of the WL UPD residuals for Solution A (left), Solution B (middle), and Solution C (right).

pseudo-range variations, and the WL UPD difference between BDS-2 and BDS-3. The histograms of the WL UPD residuals for Solution A, Solution B, and Solution C are shown in Fig. 6. The WL UPD residuals estimated by all three strategies obey a normal distribution, and solution C gives a smaller deviation than the other strategies. The percentages of WL UPD residuals for Solution A, Solution B, and Solution C that are less than 0.25 cycles

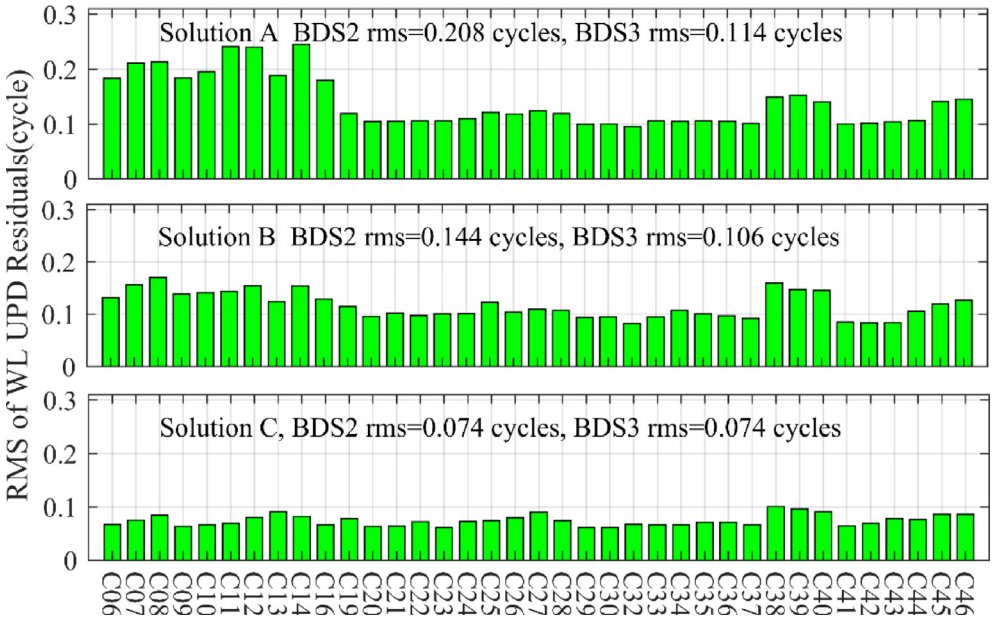

Fig. 7. RMS value of WL UPD residuals for each BDS satellite, during DOY 213–242,2021.

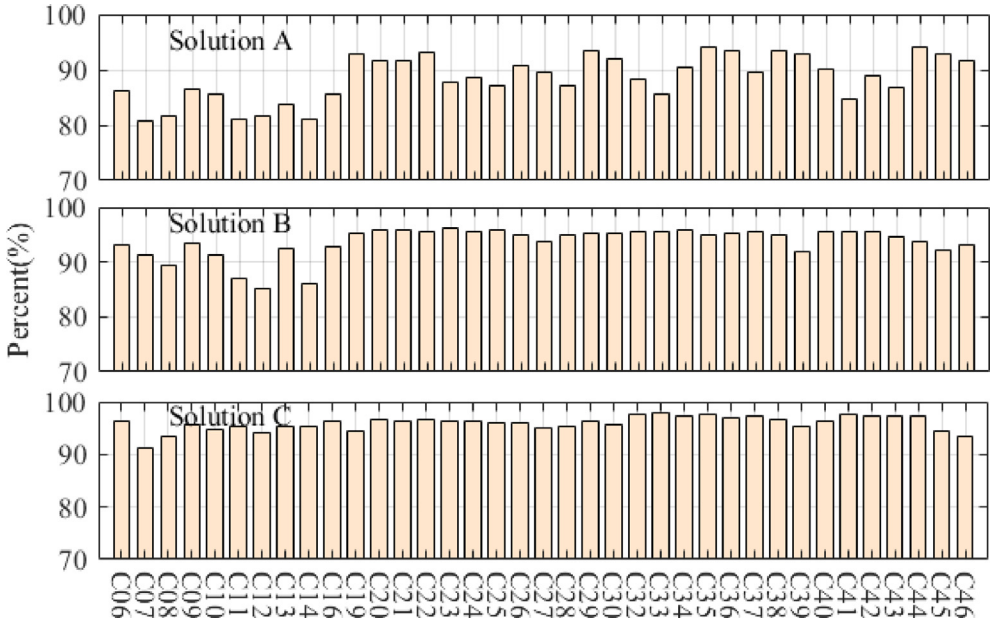

Fig. 8. Average data utilization rate of WL ambiguity for each BDS satellite, during DOY 213–242, 2021.

are 89.71 %, 95.11 %, and 99.99 %, respectively. This indicates that the BDS WL UPD estimation strategy used by solution C is the best.

In addition, the RMS values of WL UPD residuals over the 30 days for each BDS satellite are computed and are shown in Fig. 7. The results show that the average RMS of WL UPD residuals for Solution A, Solution B, and Solution C are 0.14, 0.12, and 0.07 cycles, respectively. Comparing results from Solution A with those from Solution B, it can be concluded that correcting for the satellite-induced code pseudo-range variations can significantly decrease the WL UPD residuals of BDS-2 satellites. In addition, when the WL UPD difference between BDS-2 and BDS-3 is not considered, the BDS-2 average WL UPD residuals in solution B are greater than the BDS-3 average value. This is caused by two factors: (1) the majority of BDS-3 satellites are MEO satellites, hence there are more stations tracking BDS-3 satellites than tracking BDS-2 satellites; and (2) there are 27 satellites in BDS-3 compared to 10 satellites in BDS-2. As a result, when performing the UPD adjusted leveling estimation, BDS-3 has more observations than BDS-2, hence the receiver WL

UPD is closer to the BDS-3 value. According to Solution C, when considering the WL UPD difference between BDS-2 and BDS-3, the WL UPD residuals are essentially at the same level for all BDS satellites.

Fig. 8 gives the 30-day average utilization rate of WL ambiguity for each BDS satellite. The results of Solution A show that the ambiguity utilization rate of BDS-2 satellites is basically below 85 %, without correction of the satellite-induced code pseudo-range variations. As can be seen from the results of Solution C, when the WL UPD difference between BDS-2 and BDS-3 is estimated, the average data utilization is increased to over 90 % for all BDS satellites.

4.2. Results of NL UPD

The RMS values of NL UPD residuals over the 30 days for all the BDS satellites are shown in Fig. 9. The average RMS of NL UPD residuals for Solution A, Solution B, and Solution C are 0.12, 0.10, and 0.09 cycles, respectively. The

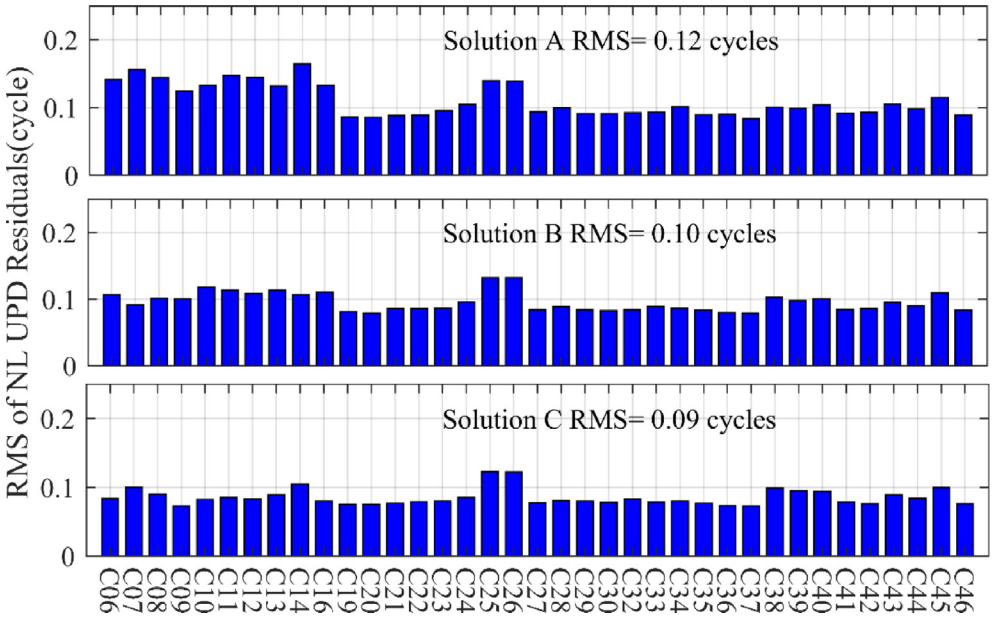

Fig. 9. RMS values of NL UPD residuals for each BDS satellite, during DOY 213–242, 2021.

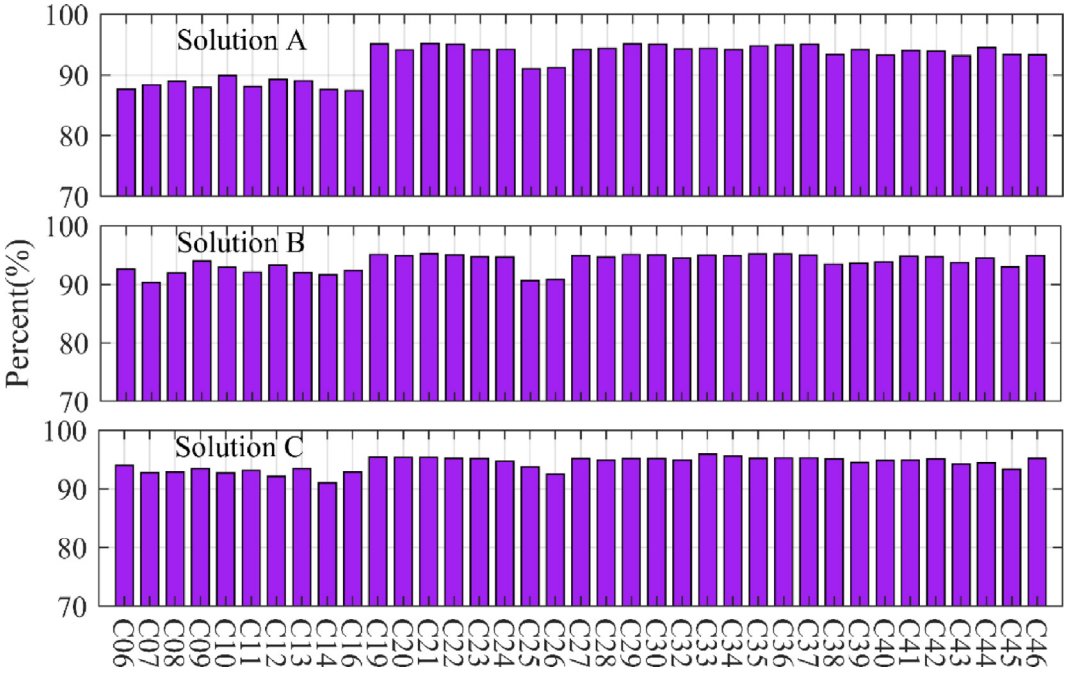

Fig. 10. Average data utilization rate of NL ambiguity for each BDS satellite, during DOY 213–242, 2021.

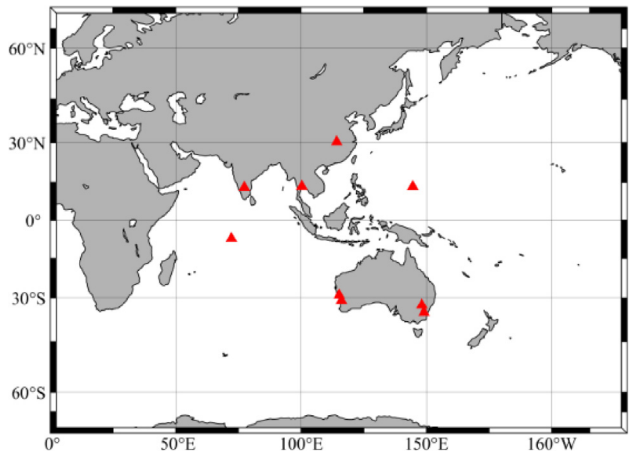

Fig. 11. Distribution of the 10 MGEX stations.

results from Solution C are optimal, and prove that correcting the satellite-induced code pseudo-range variations and estimating ISBs are beneficial for BDS NL UPD estimation.

Fig. 10 shows the 30-day average utilization rate of NL ambiguity for each BDS satellite. The ambiguity utilization rate of BDS-2 satellites is basically below 95 %, without correction of the satellite-induced code pseudo-range variations. After correcting for these variations, the NL ambiguity utilization of the BDS-2 satellites in Solution B improves to over 90 %. Moreover, the results of Solution C indicate that the NL ambiguity utilization rate of all BDS satellites can be maximized when the ISBs between BDS-2 and BDS-3 are estimated.

5. BDS PPP/PPP-AR results and analysis

In this section, to assess the quality of the estimated BDS UPDs and ISBs, 10 MGEX stations are used to analyze BDS PPP and BDS PPP-AR, these stations distributed around the Asia-Pacific region thus to observe more BDS-2 and BDS-3 satellites. The timespan for data calculation is DOY 213–242, 2021. Fig. 11 shows the distribution of the 10 MGEX stations.

The performance of PPP and PPP-AR are assessed in terms of convergence time and positioning accuracy. In addition, static and kinematic PPP/PPP-AR are processed. In this study, the positioning result is considered to have converged when the absolute values of the positioning errors are lower than the threshold for the consecutive ten epochs. The thresholds of the horizontal and vertical directions are set to 5, 10 cm for static PPP, and 10, 20 cm for kinematic PPP, respectively. The reference coordinates of the stations are derived from the SNX products provided by IGS. For ambiguity resolution, the bootstrap method is applied to fix the WL ambiguities, while a partial search strategy based on the LAMBDA method is used to fix the NL ambiguities (Li et al., 2013; Teunissen, 2002; Xiao et al., 2019).

5.1. RMS for static and kinematic PPP solutions

To evaluate the influence of ISB on the joint BDS PPP and PPP-AR, the positioning result (*)–NO indicates that the ISB is not estimated, and (*)-EST indicates that the ISB is estimated. Fig. 12 presents the epoch series of GUAM on DOY 213, 2021 in the North (N), East (E),

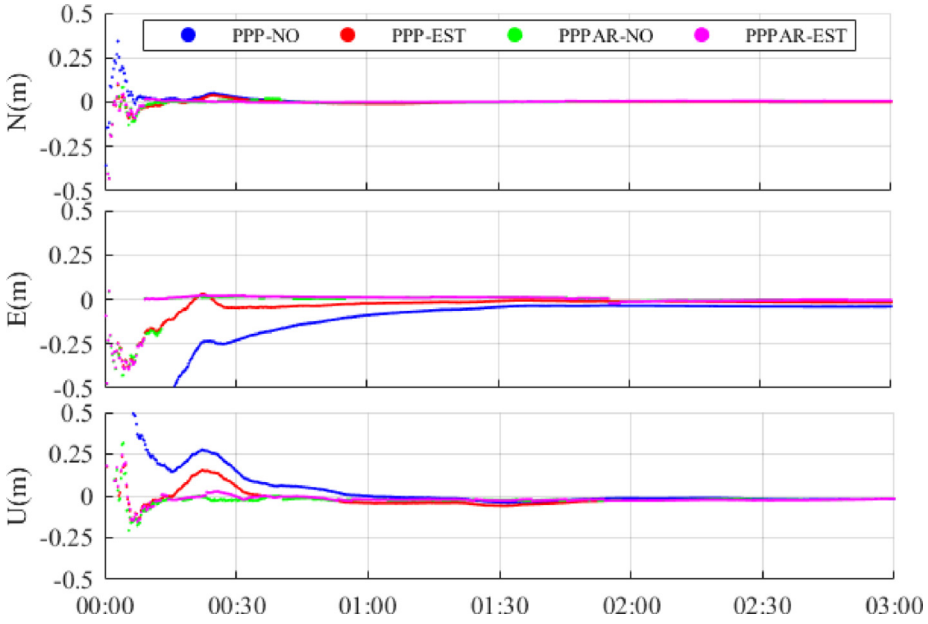

Fig. 12. Static PPP and PPP-AR solutions of station GUAM on DOY 213, 2021.

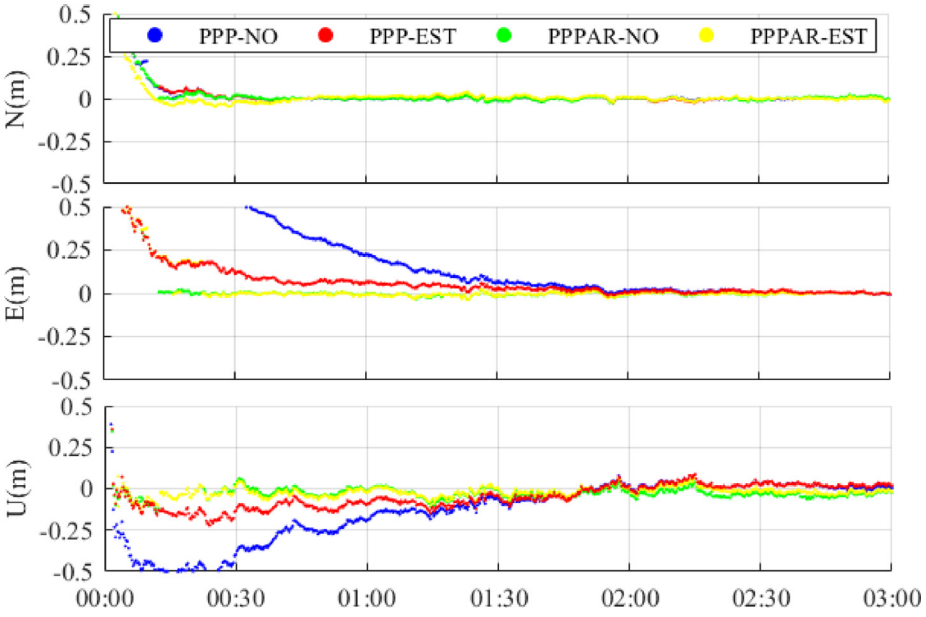

Fig. 13. Kinematic PPP and PPP-AR solutions of station PARK on DOY 215, 2021.

Table 4
Average RMS for static/kinematic PPP and PPP-AR (unit: cm).

Mode	ISB-NO			ISB-EST		
	N	E	U	N	E	U
PPP static	0.55	0.62	1.56	0.57	0.61	1.56
PPP-AR static	0.51	0.44	1.44	0.52	0.45	1.41
PPP kinematic	1.51	1.97	4.66	1.57	1.95	4.67
PPP-AR kinematic	1.43	1.61	4.59	1.46	1.59	4.56

and Up (U) directions for BDS static PPP and BDS static PPP-AR. Fig. 12 shows that the ISB parameter could affect the convergence speed of static PPP, but the final positioning accuracy is consistent for the NISB and YISB modes in the N, E, and U directions. Additionally, PPP-AR can greatly reduce convergence time, which demonstrates the reliability of the BDS UPD estimated in Section 4.

In addition, the kinematic PPP and PPP-AR solutions of PARK on DOY 215, 2021 are shown in Fig. 13. The introduction of ISB parameter also accelerates the convergence speed of kinematic PPP, and the positioning

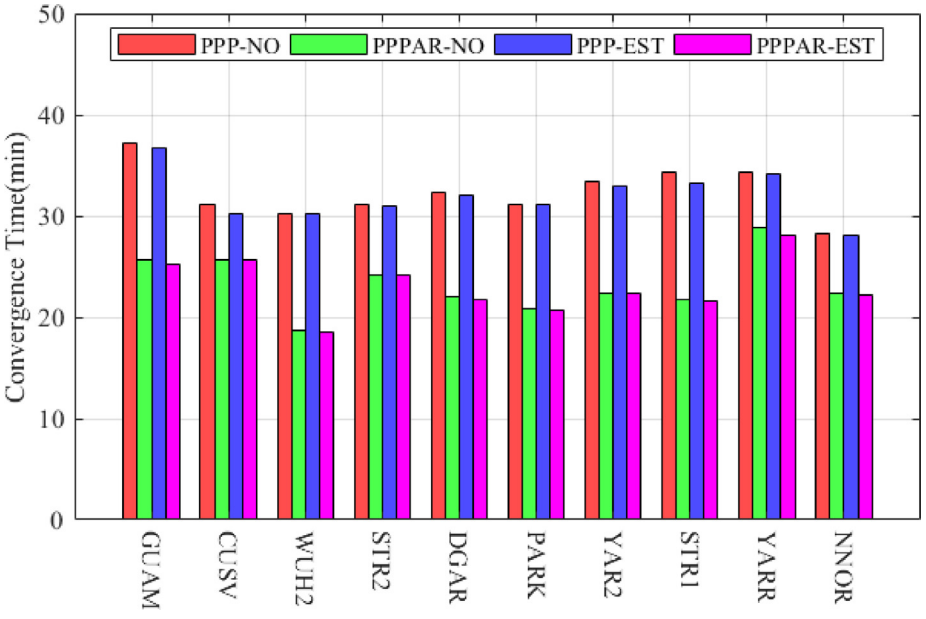

Fig. 14. Mean convergence time of static PPP and PPP-AR solutions for 10 stations.

accuracy after convergence also tends to be consistent, which is like the static PPP. Comparing the PPP float solution and fixed solution, the improvement of convergence speed is more obvious in the E and U directions.

Table 4 shows the statistical results of the average RMS of the final positioning error of the BDS static and kinematic PPP and PPP-AR for the 10 stations. The effect of the ISB parameter on the final positioning error of static PPP and PPP-AR is less than 1 mm. In the N, E, and U directions, the RMS values of static BDS PPP-AR are 0.5, 0.4, and 1.4 cm, respectively; in the N, E, and U directions, the RMS values of static PPP are 0.6, 0.6 and 1.6 cm, respectively. Like the static PPP, the ISB parameter has essentially no effect on positioning accuracy after convergence of the kinematic PPP. Compared with BDS kinematic PPP, the positioning accuracy of BDS PPP-AR is improved, and the RMS values of BDS kinematic PPP-AR in the N, E, and U directions are 1.5, 1.6, and 4.6 cm, respectively. Compared with BDS PPP, the positioning accuracy of BDS PPP-AR is significantly improved, especially in the E direction.

5.2. Convergence time

Fig. 14 shows the mean convergence time of the static PPP and PPP-AR for the ten MGEX stations from DOY 213–242, 2021. It can be seen that the introduction of the ISB parameter does not make any significant improvement to the convergence speed of the BDS PPP and BDS PPP-AR. The mean convergence time of BDS static PPP is 31.6 min for 10 stations, and the mean convergence time of BDS static PPP-AR is 22.33 min. Compared with the PPP result, the convergence time of PPP-AR is shortened by 29.3 %.

Fig. 15 shows the mean convergence time of the kinematic PPP and PPP-AR for the ten MGEX stations. As

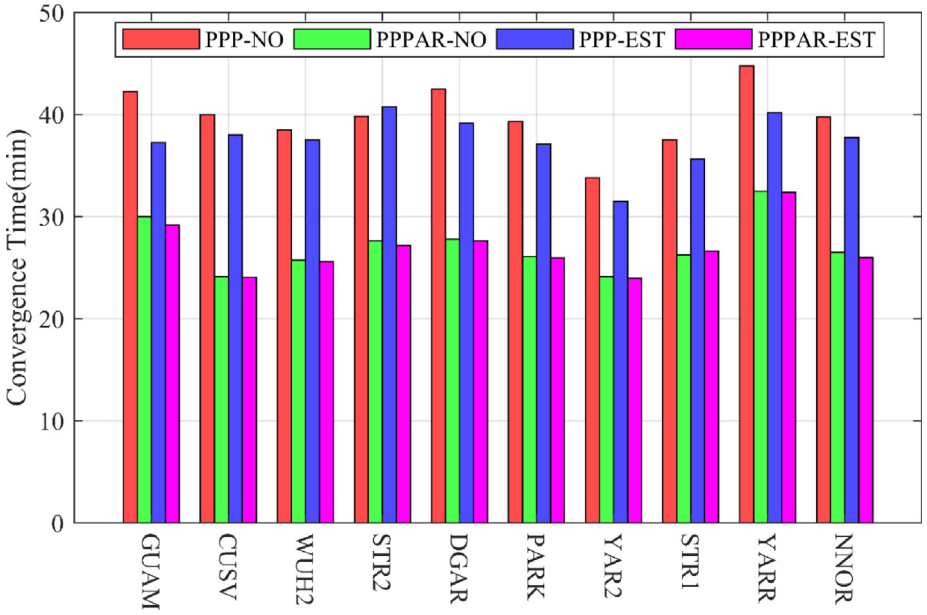

Fig. 15. Mean convergence time of kinematic PPP and PPP-AR solutions for 10 stations.

Table 5
Ambiguity fix rate for static and kinematic PPPAR for 10 stations (unit: %).

Site	Static			Kinematic		
	ISB-NO	ISB-EST	Improvement (%)	ISB-NO	ISB-EST	Improvement(%)
GUAM	94.56	94.51	−0.05	90.30	90.38	0.08
CUSV	93.57	95.82	2.40	92.63	93.00	0.39
WUH2	95.99	95.55	−0.45	93.73	93.78	0.05
STR2	95.96	94.17	−1.86	92.27	91.73	−0.58
DGAR	95.77	96.32	0.57	92.31	92.34	0.03
PARK	94.73	94.47	−0.27	93.69	93.57	−0.12
YAR2	95.90	95.43	−0.4	92.18	92.23	0.05
STR1	93.95	94.49	0.57	93.85	94.01	0.17
YARR	95.37	95.36	−0.01	92.42	92.23	−0.20
NNOR	93.20	94.24	1.11	92.42	92.43	0.01
Mean	94.90	95.03	0.13	92.58	92.57	−0.01

can be seen in Fig. 14, the ISB parameter could shorten the convergence time of kinematic PPP, but its impact on PPP-AR convergence time is not significant. In addition, the convergence time of BDS PPP-AR is also shortened compared with float PPP solutions. The mean convergence times of BDS kinematic PPP and PPP-AR are 37.57 min and 26.74 min, respectively, and the convergence time of PPP-AR is shortened by 28.7 %.

5.3. PPP-AR Ambiguity-fixed success rate

The ambiguity-fixed rate can be calculated using the number of ambiguity-fixed solutions among the total number of ambiguity parameters. In this research, a successful ambiguity-fixed solution is defined when the ambiguity is fixed in PPP-AR, the position error in each direction is lower than that of the float PPP, and the positioning error is less than 10 cm. The ambiguity-fixed rates are shown in Table 5.

According to the results shown in Table 5, when the ISB is not estimated, the average ambiguity fix rates for static and kinematic PPP-AR are 94.90 % and 92.58 %, respectively. When the ISB is estimated, the ambiguity fix rates for static and kinematic PPP-AR are 95.03 % and 92.57 %, respectively. This indicates that adding the ISB parameter does not reduce the ambiguity-fixed rate.

of the BDS PPP-AR.

6. Conclusions and discussions

BDS PPP-AR has not yet been widely investigated and applied. In this research, we considered the ISBs between the BDS-2 and BDS-3 systems in UPD estimation. To estimate the ISBs between BDS-2 and BDS-3 and the BDS UPD products, we collected observation data from 130 globally distributed MGEX stations over a period of one month. The characteristics of ISBs and the quality of BDS UPDs were analyzed and evaluated. In addition, 10 MGEX stations distributed around the Asia-Pacific region were used to analyze BDS PPP and BDS PPP-AR from the perspectives of positioning accuracy, convergence time, and the ambiguity-fixed rate. Here, some conclusions are presented as evidence for the application of BDS-2 and BDS-3 joint processing:

Firstly, the ISB value is related to the type and version of the receiver, and the ISBs of stations with receivers of the same type are similar. The ISB parameter can be regarded as a constant value within a given day, and the mean STD values of ISBs for different types of receivers over the course of a month are generally within 0.2 m.

Secondly, correcting for the satellite-induced code pseudo-range variations can significantly decrease the WL UPD residuals of BDS-2 satellites. Additionally, when considering the ISBs and WL UPD differences between BDS-2 and BDS-3, the WL and NL UPD residuals are essentially at the same level for all BDS satellites. Moreover, the average data utilization rates of WL and NL ambiguity increase to over 90 %.

Furthermore, our validation results show that, in terms of convergence speed and positioning accuracy, performance is significantly improved with the BDS PPP-AR solution. In addition, the results indicate that ISB can improve the convergence speed of static and kinematic PPP, but it can be disregarded in PPP-AR.

Overall, the ISB and code pseudo-range variations improve the estimation of the UPDs in the network solution. Therefore, we suggest the ISB need to be estimated when estimating UPD products on the network side. However, the effect for the user in float PPP and PPPAR is not significant. It should be also pointed out that we only use BDS satellites here; as such, the multi-GNSS PPP-AR should be further analyzed. In addition, multi-frequency BDS UPD estimation and PPP-AR represent further areas to be investigated.

Declaration of Competing Interest

The authors declare that they have no known competing financial interests or personal relationships that could have appeared to influence the work reported in this paper.

Acknowledgments

This work is mainly funded by Program of Shanghai Academic/Technology Research Leader; The Key R&D Program of Guangdong province of China (Grant No. 2018B030325001); National Natural Science Foundation of China (No. 11673050); National Key R&D Program of China (No. 2018YFB0504300); Opening Project of Shanghai Key Laboratory of Space Navigation and Positioning Techniques (No. 202114); National Natural Science Foundation of China, Grant/Award Number: 41904034. We thank the data provided by the International GNSS Service (IGS).

References

Boisits, J., Glaner, M., Weber, R., 2020. Regiomontan: a regional high precision ionosphere delay model and its application in precise point positioning[J]. Sensors 20 (10), 2845.

Chen, H., Liu, X., Jiang, W., et al., 2021. Preliminary analysis and evaluation of BDS-2/BDS-3 precise point positioning[J]. Adv. Space Res. 68 (10), 4113–4128.

Chen, J., Zhang, Y., Wang, J., et al., 2015. A simplified and unified model of multi-GNSS precise point positioning[J]. Adv. Space Res. 55 (1), 125–134.

Chen, J., Zhang, Y., Yu, C., et al., 2022. Models and performance of SBAS and PPP of BDS[J]. Satellite Navig. 3 (1), 1–14.

Collins J P, Lahaye F, Heroux P, Bisnath S. Precise point positioning with ambiguity resolution using the decoupled clock model. In: Proceedings

of ION GNSS 21st international technical meeting of the satellite division, 2008, Savannah, US, pp 1315-1322.

Ge, M., Gendt, G., Rothacher, M., Shi, C., Liu, J., 2008. Resolution of GPS carrier-phase ambiguities in Precise Point Positioning (PPP) with daily observations[J]. J. Geod. 82 (7), 389–399.

Geng, J., Shi, C., Ge, M., Dodson, A., Lou, Y., Zhao, Q., 2012. Improving the estimation of fractional-cycle biases for ambiguity resolution in precise point positioning[J]. J. Geod. 86 (8), 579–589.

Geng, J., Li, X., Zhao, Q., et al., 2019a. Inter-system PPP ambiguity resolution between GPS and BeiDou for rapid initialization[J]. J. Geod. 93 (3), 383–398.

Geng, J., Guo, J., Chang, H., et al., 2019b. Toward global instantaneous decimeter-level positioning using tightly coupled multi-constellation and multi-frequency GNSS[J]. J. Geod. 93 (7), 977–991.

Glaner, M., Weber, R., 2021. PPP with integer ambiguity resolution for GPS and Galileo using satellite products from different analysis centers [J]. GPS Solut. 25 (3), 1–13.

Hu, J., Li, P., Zhang, X., et al., 2022. Precise point positioning with BDS-2 and BDS-3 constellations: ambiguity resolution and positioning comparison[J]. Adv. Space Res.

Jiao, G., Song, S., Jiao, W., 2020. Improving BDS-2 and BDS-3 joint precise point positioning with time delay bias estimation. Measur. Sci. Technol. [J] 31 025001.

Kouba, J., Héroux, P., 2001. Precise point positioning using IGS orbit and clock products[J]. GPS Solut. 5 (2), 12–28.

Laurichesse, D., Mercier, F., Berthias, J.P., Broca, P., Cerri, L., 2009. Integer ambiguity resolution on undifferenced GPS phase measurements and its application to PPP and satellite precise orbit determination. Navigation 56, 135–149.

Li, X., Li, X., Liu, G., Yuan, Y., Freeshah, M., Zhang, K., Zhou, F., 2020. BDS multi-frequency PPP ambiguity resolution with new B2a/B2b/B2a+ b signals and legacy B1I/B3I signals[J]. J. Geod. 94 (10), 1–15.

Li, B., Verhagen, S., Teunissen, P.J.G., 2013. GNSS integer ambiguity estimation and evaluation: LAMBDA and Ps-LAMBDA. In: China Satellite Navigation Conference (CSNC) 2013 Proceedings. Springer, Berlin, Heidelberg, pp. 291–301.

Liu, X., Jiang, W., Li, Z., et al., 2019. Comparison of convergence time and positioning accuracy among BDS, GPS and BDS/GPS precise point positioning with ambiguity resolution[J]. Adv. Space Res. 63 (11), 3489–3504.

Lou, Y., Zheng, F., Gu, S., et al., 2016. Multi-GNSS precise point positioning with raw single-frequency and dual-frequency measurement models[J]. GPS Solut. 20 (4), 849–862.

Lou, Y., Gong, X., Gu, S., et al., 2017. The characteristic and effect of code bias variations of BeiDou[J]. Geomat. Information Sci. Wuhan Univ. 42 (8), 1040–1046.

Melbourne W.G (1985) The Case for Ranging in GPS-based Geodetic Systems. Proceedings of 1st International Symposium on Precise Positioning with the Global Positioning System, Rockville, MD, USA, 15–19 April 1985, 373–386.

Meng, L., Wang, J., Chen, J., et al., 2020. Extended geometry and probability model for GNSS+ constellation performance evaluation [J]. Remote Sensing 12 (16), 2560.

Qin, W., Ge, Y., Zhang, Z., et al., 2020. Accounting BDS3–BDS2 inter-system biases for precise time transfer. Measurement [J] 156 107566.

Qu, L., Du, M., Wang, J., et al., 2019. Precise point positioning ambiguity resolution by integrating BDS-3e into BDS-2 and GPS[J]. GPS Solut. 23 (3), 1–11.

Shi, C., Hu, Y., Zheng, F., et al., 2022. Accounting for BDS-2/BDS-3 inter-system biases in PPP and RTK models[J]. Adv. Space Res.

Song Z, Chen J, Wang B, et al. Analysis and modeling of the inter-system bias between BDS-2 and BDS-3[C]//China Satellite Navigation Conference. Springer, Singapore, 2020: 279-289.

Teunissen P, Joosten P, Tiberius C. A comparison of TCAR, CIR and LAMBDA GNSS ambiguity resolution. In: Proceedings of the 15th International Technical Meeting of the Satellite Division of the Institute of Navigation (ION GPS 2002), 200, 2799-2808.

Wanninger, L., Beer, S., 2015. BeiDou satellite-induced code pseudorange variations: diagnosis and therapy[J]. GPS Solut. 19 (4), 639–648.

Wubbena G (1985) Software developments for geodetic positioning with GPS using TI-4100 code and carrier measurements. Proceedings of the First International Symposium on Precise Positioning with the Global Positioning System, Maryland, 15-19.

Xiao, G., Li, P., Gao, Y., et al., 2019. A unified model for multi-frequency PPP ambiguity resolution and test results with Galileo and BeiDou triple-frequency observations[J]. Remote Sensing 11 (2), 116.

Yang, Y., Li, J., Xu, J., Tang, J., Guo, H., He, H., 2011. Contribution of the compass satellite navigation system to global PNT users. Chin. Sci. Bull. 56, 2813–2819.

Yang, Y.X., Mao, Y., Sun, B.J., 2020. Basic performance and future developments of BeiDou global navigation satellite system. Satell. Navig. 1, 1.

Zhao, W., Chen, H., Gao, Y., et al., 2020. Evaluation of inter-system bias between BDS-2 and BDS-3 satellites and its impact on precise point positioning[J]. Remote Sensing 12 (14), 2185.

Zhou, F., Dong, D., Li, P., Li, X., Schuh, H., 2019. Influence of stochastic modeling for inter-system biases on multi-GNSS undifferenced and uncombined precise point positioning[J]. GPS Solut. 23 (3), 59.

Zumberge, J.F., Heflin, M.B., Jefferson, D.C., et al., 1997. Precise point positioning for the efficient and robust analysis of GPS data from large networks[J]. J. Geophys. Res. Solid Earth 102 (B3), 5005–5017.